Eur. Phys. J. B **19**, 357–362 (2001)

THE EUROPEAN PHYSICAL JOURNAL B

EDP Sciences

Nanosize patterns as reference structures for macroscopic transport properties and vortex phases in YBCO films

E. Mezzetti[1,a], A. Chiodoni[1], R. Gerbaldo[1], G. Ghigo[1], L. Gozzelino[1], B. Minetti[1], C. Camerlingo[2], and C. Giannini[3]

[1] INFM - UdR Torino-Politecnico; INFN - Sez. Torino, Politecnico di Torino, c.so Duca degli Abruzzi 24, 10129 Torino, Italy
[2] Istituto di Cibernetica del Consiglio Nazionale delle Ricerche, Via Toiano 6, 80072 Arco Felice, Italy
[3] PaSTIS-CNRSM, SS 7 Appia km.712, 72100 Brindisi, Italy

Received 16 October 2000 and Received in final form 28 November 2000

Abstract. This paper reports on the striking correlation between nanosize mosaic domain walls in YBCO films and 1D rows of parallel Josephson junctions, determining the J_c *vs.* B curves. From X-ray data analysis, it results that the average "hidden" domain wall, faceted at a nanometric scale, is almost mimicking the Josephson Junction (JJ) 1D array. The assumption that the JJs and the domain-wall arrays are coincident, enables to find out the particular scaling field, making the J_c *vs.* B curves independent of temperature. This scaling field can be interpreted in terms of the Josephson nature of the transport current across these particular patterns in the intermediate temperature range. By means of our model it is also possible to calculate two asymptotic behaviors of the pinning force as a function of field, for low and high fields, respectively. These behaviors are punctually repeated by the experimental results in the same asymptotic limit, so that two corresponding vortex regimes are clearly pointed out. All results can be interpreted by concluding that in the intermediate temperature range, the strong pinning observed in high quality YBCO films is due to the Josephson Junctions average patterns. These patterns are the counterpart related to the transport mechanisms of "hidden" structural nano-domains.

PACS. 74.76.Bz High-T_c films – 74.60.Jg Critical currents – 74.50.+r Proximity effects, weak links, tunneling phenomena, and Josephson effects – 74.60.Ge Flux pinning, flux creep, and flux-line lattice dynamics

1 Introduction

The particular behavior of the critical current density as a function of field and temperature in high temperature superconducting thin films with respect to single crystals has been widely investigated in past and recent papers. The central questions concerns the reason why good quality films exhibit critical current density higher than single crystals, why the J_c *vs.* log$B$ curves show plateau-like features (a typical example is shown in Fig. 1), what kind of pinning mechanisms can explain the variation of the curves with temperature [1–4]. The morphology of the film is generally assumed to be responsible for the observed trends and in particular for the strong pinning. Nanosize dislocations with columnar character were found and described in detail [5,6].

From another point of view, a nanosize JJ array is considered as the basic structure accounting for the experimental data [7–11]. In the framework of this second scenario, a quantitative account of the experimental trends in the intermediate range of temperature was found. In particular, the model is based on an average 1D row of "hidden" Josephson Junction (JJ) which can be visualized as a faceted wall between contiguous domains [12,13]. The JJ exhibit statistical distributed nano-length. In order to take into account the inter-vortex magnetic interaction, a suitable "magnetic thickness" of the junctions has been considered [14]. The fitting of the data by means of our model, enables to evaluate the order of magnitude of the average JJ length as well as the statistical length-distribution shape [15].

In this paper we first of all focus on X-ray measurements. The key point of the study consists in showing that the film plane is laced by a mosaic of nanosize structural domains (see the sketch in the inset of Fig. 1). Similarly, the structural domains reflect the presence of c-axis deep dislocations, which accommodate lattice mismatches across the domain boundaries. Very significantly, the average length scale and length distribution of the domain walls almost replay (under reasonable assumptions) the lengths and length distributions of the JJs. The transport current is thus driven across the mentioned patterns.

The correspondence between the structural network and the JJ network enables to determine the value of a parameter ζ accounting for the particular domain structure between vortices in a given film [15]. This parameter

[a] e-mail: mezzetti@polito.it

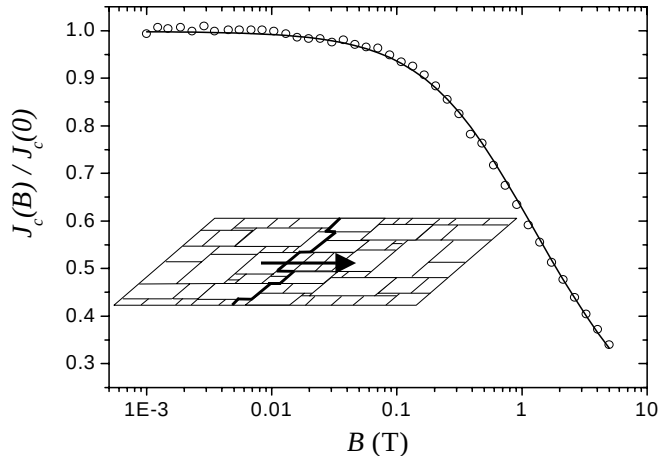

Fig. 1. Typical critical current density *vs.* applied magnetic field, as deduced from the susceptibility measurement. J_c experimental data at $T = 28$ K (symbols), normalized to the zero- field value $J_c(0) = 2.15 \times 10^{10}$ A/m^2, are fitted (solid line) by means of equation (3). In the inset, a schematic view of the JJ network is shown (the arrow indicate the current path).

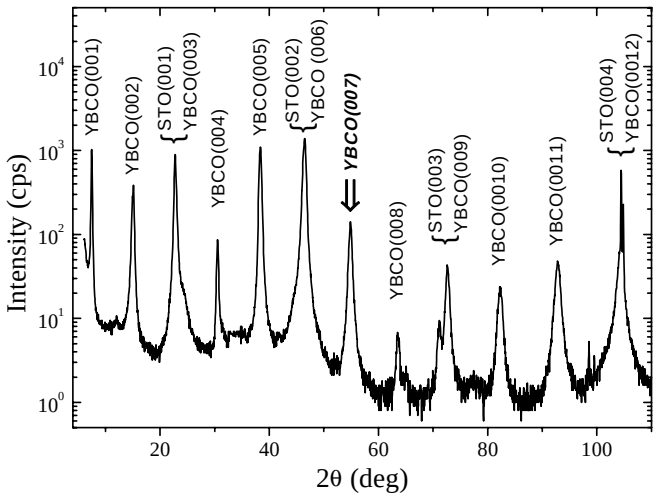

Fig. 2. X-ray diffraction profile measured on the YBCO film grown on top of the (001)-oriented STO substrate.

results to be a key one because it allows to find out in a straightforward way the scaling field B_0 making the $J_c/J_c(0)$ *vs.* B/B_0 curves independent of temperature. Therefore the model enables to account for the quite particular dependence of the J_c *vs.* B curves on temperature in YBCO films.

Finally the model is checked by considering the pinning force asymptotic behaviors to verify that the asymptotic curves are coincident with the experimental ones in the extreme limits. In the intermediate range of temperature, two main vortex regimes corresponding to those asymptotic behaviors emerge. The results can be interpreted by saying that the JJs can shrink vortices inside and optimally pin them up to a maximum field [16]. Above this field no more vortices can be pinned.

These findings imply that the magnetic transport properties of high T_c films in the intermediate temperature range (it means in the range where the nanostructure length-scale is comparable with the fluxon dimensions) are governed by nano-faceted domains walls [17]. The facet average-length and distribution is measurable. The strong pinning in the films is provided by "useful" JJs, which represent the transport counterpart of the structural patterns.

2 Experimental

The $YBa_2Cu_3O_{7-\delta}$ films were fabricated by dc sputtering from inverted cylindrical magnetron on $SrTiO_3$ (STO) substrates. The growth procedure has been described elsewhere [10]. The film nucleate on the $SrTiO_3$ substrate in the form of *c*-axis oriented texture [18]. X-ray φ-map measurements [18] indicate that the film orientation, with *c*-axis oriented along the normal of film surface and the *a*-axis oriented in plane along the cubic cell side, is not dependent on whatever substructure we could observe.

In order to have more insight about the structures up to a nanometric scale, the samples were characterized by a further XRD analysis by using a Philips-1880 diffractometer equipped with a Cu target as X-ray source, a 1/30° collimation slit and a 0.1 mm receiving slit. Figure 2 shows the X-ray diffraction profile measured, in a coupled $\theta - 2\theta$ movement, on the YBCO film, grown on top of the (001)-oriented STO substrate. The spectrum shows several peaks belonging to the (00l) family planes of the YBCO and STO crystal lattices. This spectrum provides a further confirmation that the YBCO film shows a good *c*-axis orientation. Critical current density values have been extracted from susceptibility measurements by means of the procedure described in reference [10].

3 Models

3.1 XRD analysis

A statistical model was used to analyze the X-ray data through a line shape fitting procedure based on a Monte Carlo approach. This model describes the broadening of the diffraction peaks as the consequence of the frequency distribution of the grain size [19]. The inset of Figure 3a shows the fitting results obtained from the analysis of the YBCO (007) peak indicated by the arrow in Figure 2. This analysis was performed on a single peak. In principle we could have chosen any of the measured order reflections. The reflections at very low angles are the best for the determination of the grain size distribution because the lower is the scattering angle the less important are the contributions to the peak lineshape due to microstrain or structural defects. Nevertheless, working on peaks collected at very low glancing angles has the drawback that background effects are detrimental to peak analysis. In conclusions, in order to obtain the best accuracy in the lineshape fit, we definitively worked on the (007) peak.

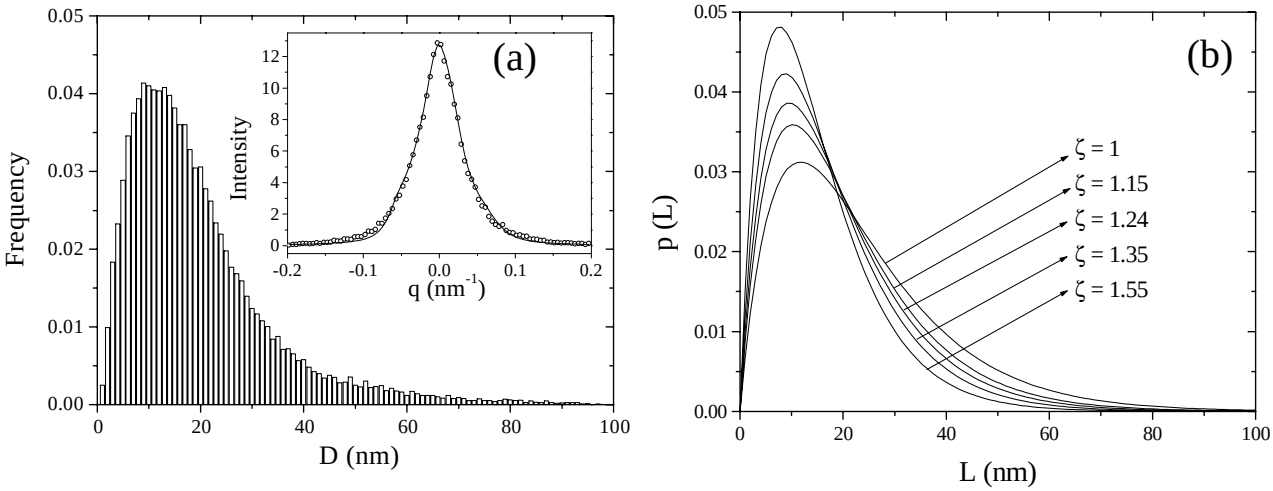

Fig. 3. The inset of (a) shows the fitting results obtained from the analysis of the YBCO (007) peak, indicated by the arrow in Figure 2. The complete frequency distribution of the grain size is shown in the main panel (a). The junction-length distributions resulting from the fit reported in Figure 1 for different ζ values is reported in (b).

It results that nano domains are present. In Figure 1 (inset) a mosaic-like representation of a multi-domain pattern is given, just to provide a visual support to the text. The average domain-size value, as derived from the previously mentioned statistical analysis, is 19 ± 3 nm, and the complete frequency distribution of the domain length-scale $p(D)$ is represented in Figure 3a.

The analysis allows putting in evidence a "hidden" [10] granularity across the films. It means that this particular granularity does not necessarily imply "weak links", in the usual meaning of the term, on the contrary it accounts for "strong links", like those observed in bicrystals when the misalignment angle is very small [12,20].

3.2 Transport current

The critical current of the array of parallel uniform short JJs of different lengths L, accounting for the particular shape of J_c *vs.* B curves, can be written as

$$J_c(B) = J_c(0) \int_0^\infty \mathrm{d}\, L\, p(L) \Big| \frac{\sin(\pi B \Lambda_0 L/\Phi_0)}{\pi B \Lambda_0 L/\Phi_0} \Big| \qquad (1)$$

where $p(L)$ is the statistical length distribution of the junctions and Λ_0 is a very crucial field- dependent "magnetic thickness" [14], that in the present case is assumed to be proportional to the mean vortex distance a_0: $\Lambda_0 = \zeta a_0$. ζ is a number of order of unity, which in a bicrystal generally depends on bulk pinning and on the geometry of the grain boundary [12]. In the context of the paper ζ will assume a more definite role. It is worthwhile emphasizing that by putting $\Lambda_0 = \zeta a_0$ instead of $\Lambda_0 = d + 2\lambda_L$ in (1), we account for the experimental evidence that it is impossible to fit the experimental curves by a superposition of usual Fraunhofer patterns with whatever statistical distribution of lengths. We choose the very general distribution

$$p(L) = \frac{\mu^\nu}{\Gamma(\nu)} L^{\nu-1} \mathrm{e}^{-\mu L} \qquad (2)$$

where the mean value $\langle L \rangle$ and the variance of the distribution σ_L^2 are related to μ and ν by

$$\mu = \langle L \rangle / \sigma_L^2 \qquad \nu = (\langle L \rangle / \sigma_L)^2.$$

Thus (1) assumes the form

$$J_c(B) = J_c(0) \frac{1}{\Gamma(\nu) q \sqrt{B}} \int_0^\infty x^{\nu-2} \mathrm{e}^{-x} \left| \sin(q\sqrt{B}x) \right| \mathrm{d}x \qquad (3)$$

where $q = \pi \zeta \langle L \rangle / (\nu \Phi_0^{1/2})$.

The theoretical curves fit quite nicely the experimental data, accounting for the plateau like feature characteristic of YBCO films in the intermediate range of temperature (a typical example is shown in Fig. 1). Moreover, the fit allows determining $\langle L \rangle \zeta$ and $\langle L \rangle / \sigma_L$ It must be stressed out that this fit does not provide the independent determination of $\langle L \rangle$, ζ and σ_L. However, in order to have a reliable picture of the order of magnitude of the involved length scales, as well as to have some insight about the expected length distribution, we plot in Figure 3b the length distribution corresponding to five tentative values of ζ. These values are chosen in a range near those expected in previous literature [12].

4 Results

4.1 Evaluation of the ζ parameter

In order to determine all physical parameters previously mentioned and in particular the values of ζ, a comparison between the carrier transport properties and the structural properties of the host materials on a nanosize gauge scale is needed.

The ζ parameter results to be a key one in the paper as outlined below. The frequency distribution of the domain size as calculated by the X-ray analysis ("structural

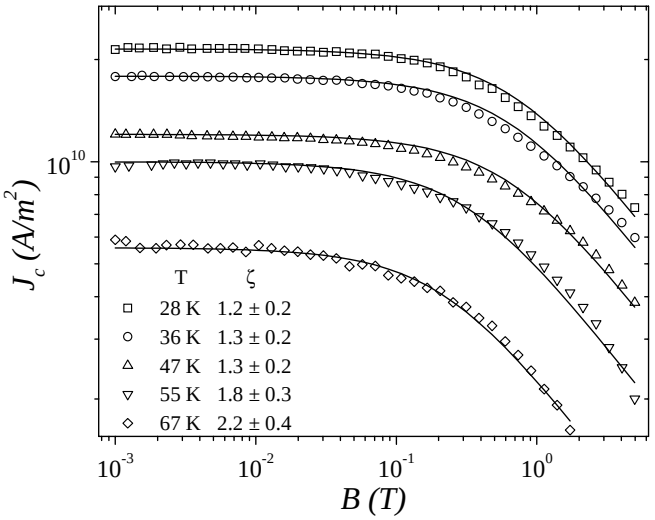

Fig. 4. Critical current density as a function of the magnetic field. Data have been fitted by (3) on the basis of the sub-grain size distribution of Figure 3. The fitting parameter ζ is reported as a function of temperature.

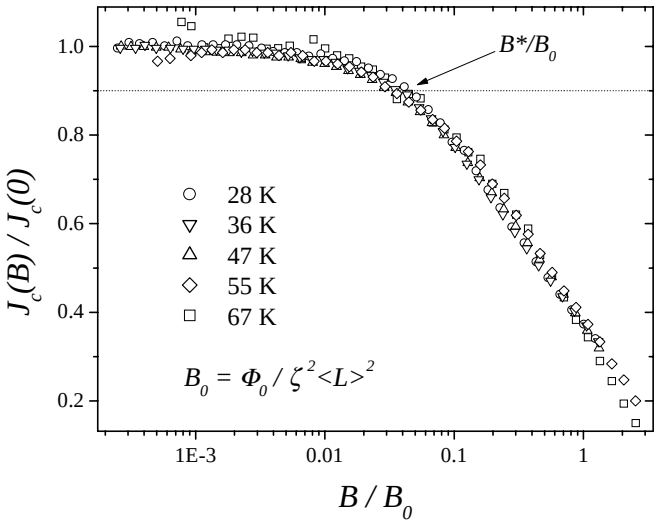

Fig. 5. Scaling of the critical current density values at different temperatures.

curve") can be very well fitted by means of the statistical distribution (2) previously used. Beside the analytical check, this fact could be easily inferred just by means of a comparative look to both Figures 3a and Figure 3b. Very significantly, the average length scale of the domains as well as the length distribution are coincident (within the experimental errors and the statistical uncertainty), with the lengths and distributions found by means of the JJ network model under realistic assumptions for the ζ parameter.

We conclude that the 1D network of JJ and the faceted multi-domain wall are two aspects of the same physical reality concerning the film nano-granularity. In fact, the structural domains reflect the presence of dislocations, which depress the order parameter. The transport current is thus driven across the mentioned patterns (Fig. 1 inset). On the basis of this correspondence, we made the hypothesis that the size distribution $p(D)$ is an ensemble representative of the junction length distribution and can be assumed as coincident with $p(L)$. We then calculated a new $p(L)$ by fitting the distribution of Figure 3a, with the same analytical expression of equation (3). This $p(L)$ can be inserted in equation (1) to obtain a new fit of the J_c *vs.* B experimental curves. In this second analysis the only free parameter left (beside $J_c(0)$) is ζ.

The results are shown in Figure 4, where the final fitting are reported. The values of ζ so obtained are reported with the experimental errors in the inset. It must be emphasized that the ζ values are drawn from the experimental data with the only assumption of the coincidence between the two mentioned distributions. The obtained values have the order of magnitude expected in literature. ζ exhibits smooth temperature dependence. Such temperature dependence can be expected, if we take into account the basic role of ζ . In fact, trough the relation $\Lambda_0 = \zeta a_0$, ζ accounts for the magnetic interactions of the pinned vortices in the real film plane. The vortices can be collectively accommodated on the basis of the nano-domain boundary geometry as well as of the length-scale of their own core. This length scale is varying with temperature in such a way that, for example, large vortices near the irreversibility line, are not sensitive to the nano domain structure of the film [10,21].

4.2 Scaling law

Figure 5 shows the normalized current density $J_c(B)/J_c(0)$ as a function of the dimensionless field $h = B/B_0$, with $B_0 = \Phi_0/(\zeta\langle L\rangle)^2$, at different temperatures. B_0 represents the first field where $J_c(B)/J_c(0)$ of a conventional JJ with virtual length $\zeta\langle L\rangle$ exhibit a minimum (one vortex entering the junction). It also determines the position of "matching fields" in a 1D array of JJ with length $\zeta\langle L\rangle$ [13,22].

The scaling aspect is quite general. In fact, the scaling behavior is also exhibited by different samples (Fig. 6). All these trends provide a further confirmation that just a JJ array is responsible for the particular feature of the J_c *vs.* B curves in films. Such network can confine vortices, thus modulating their arrangements inside the grain boundaries.

The plateau-like feature of the J_c *vs.* $\log(B)$ curves extends up to a field B^*, which can be defined in an empirical way, for example as the field where $J_c(B)/J_c(0) = 0.9$ (Fig. 5) [10]. It turns out that at all temperatures and for all samples it is $B^*/B_0 = 0.05 \pm 0.01$. This value provides an estimate of the maximum fraction of vortices trapped per unit junction of length $\zeta\langle L\rangle$, *i.e.* it represents the condition of optimal filling of the network for our films.

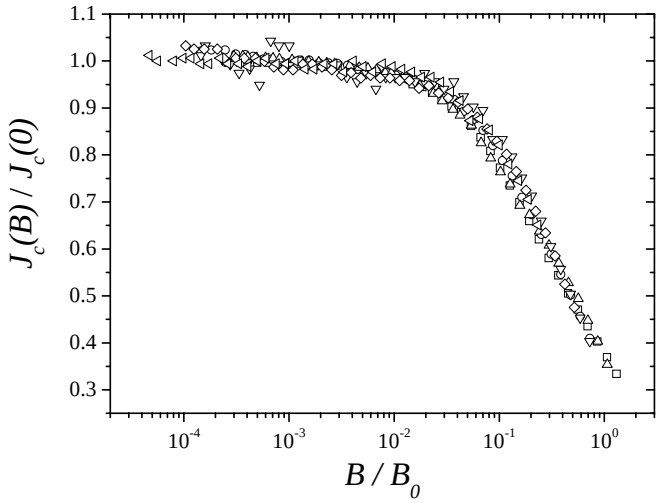

Fig. 6. Scaling of the critical current density values for six different samples at $T = 36$ K.

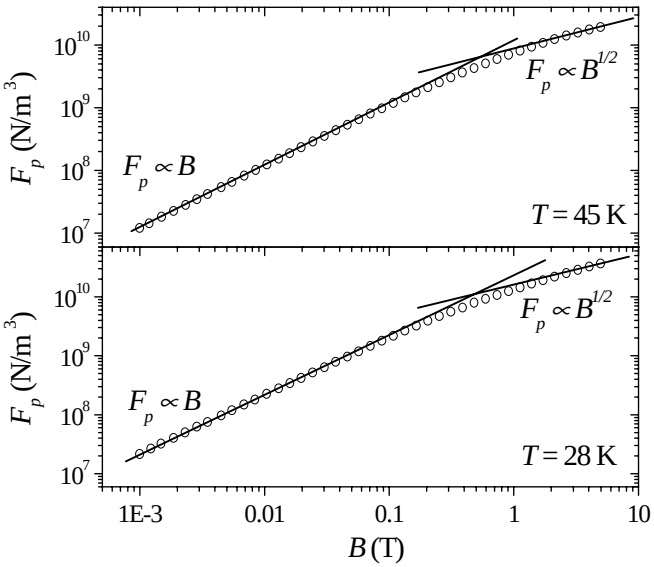

Fig. 7. Pinning force as a function of the magnetic field at two different temperatures. Two distinct behaviors can be recognized, $F_\mathrm{p} \propto B$ at low fields and $F_\mathrm{p} \propto B^{1/2}$ at high fields.

4.3 Pinning force

To assess the vortex pinning by the domain boundary network, we study the dependence of the pinning force on field, related to the domain distribution of Figure 1. Since the pinning force is defined as $F_\mathrm{p} = J_\mathrm{c}B$, its asymptotic behavior can be calculated from equation (3) up to a point phase where $J_\mathrm{c}(0)$ can be considered as constant. The limit $B \to 0$ gives straightforwardly $J_\mathrm{c}(B) = J_\mathrm{c}(0)$. The asymptotic behavior for high field is calculated in the appendix and it reads: $J_\mathrm{c}(B) \approx \sqrt{B}$ as $B \to \infty$. It results that for $B \to 0$, $F_\mathrm{p} \sim B$ and for high fields (as long as $J_\mathrm{c}(0)$ can be considered as constant) $F_\mathrm{p} \sim B^{1/2}$. In Figure 7 the two asymptotic behaviors are plotted as continuous lines, while the experimental data are represented as open symbols. The measurements, as expected by the $J_\mathrm{c}(B)$ plateau-like feature, fit well to a straight line in a log-log plot with exponent 1 at low fields; at higher fields the slope 1/2 is effectively reached.

In interpreting our data in a less quantitative, however appealing picture, we can consider the volume pinning force as proportional to the linear density of the pinned vortices, times the pinning force per unit length [23]. In the low-field range the pinning force per unit length increases as the linear vortex density increases, because in this regime all vortices entering in the unit length are supposed to find new assets and new matching conditions to the intrinsic defects lattice (first main vortex regime). This phenomenon occurs in less and less favorable conditions until a saturation regime (slope 1/2) sets up, where the pinning force per unit length becomes constant. This fact can be interpreted by claiming that no more vortices can be accommodated inside the unit length of the host defect lattice [23] (second main vortex- regime). Obviously such "continuous" model is unable to account for the discontinuous entrance of the vortices into the defect lattice itself [24]. The two asymptotic behaviors are related to a pinning mechanism in the framework of a usual language and consolidated scientific context [23].

However, using the approach focused on the role of the domain boundaries behaving as JJ, the data can be quantitatively accounted for. We argue that the two approaches are equivalent.

5 Conclusions

We have found a striking correlation between nano-sized structural patterns in the film plane and macroscopic transport current. A nano-sized JJ network of parallel junctions, contributing to the macroscopic properties is coincident with the faceted boundary between nanosize domain (structural network).

In the investigated range of temperatures the comparison enables to experimentally assess the scaling field B_0 making the curves independent of temperature. This field depends on a parameter ζ accounting for the accommodation of the vortices across the film. Once this parameter is evaluated for a given sample by means of coupled X-ray and J_c *vs.* B measurements, the curves $J_\mathrm{c}/J_\mathrm{c}(0)$ *vs.* B/B_0 collapse one over another. This scaling imply a quantitative account of the dependence of the curves on temperature.

The pinning force exhibits two asymptotic behaviors easily referred to the JJ network itself. Two corresponding asymptotic vortex phases are clearly pointed out. The network accounts for the strong domain pinning across the film.

All our results can be interpreted and summarized by saying that, in the intermediate range of temperature (it means as long as the fluxons gauge-scale is comparable to the length scale of measurable faceted domain walls) the pinning is provided by "hidden" rows of "strong" JJs.

Work partially supported by a MURST COFIN98 program (Italy) and by ASI-ARS/99/16 project. The authors wish to thank A. Barone, C. Nappi, S. Martelli and L. Tapfer for helpful discussions.

Appendix

The equation (3) can be written using the Fourier series

$$|\sin(x)| = \frac{2}{\pi}\left[1 - 2\sum_{n=1}^{\infty}\frac{\cos(2nx)}{4n^2-1}\right].$$

The critical current is then

$$J_{\rm c}(B) = J_{\rm c}(0)\frac{1}{\Gamma(\nu)q\sqrt{B}}\frac{2}{\pi}$$
$$\times\left[\int_0^{\infty} x^{\nu-2}{\rm e}^{-x}{\rm d}x - 2\sum_{n=1}^{n}\frac{\int_0^{\infty} x^{\nu-2}{\rm e}^{-x}\cos(2nq\sqrt{B}x){\rm d}x}{4n^2-1}\right].$$

The two integrations can be performed analytically (J.S. Gradshteyn, I.M. Ryzhik, *Table of Integrals, Series, and Products*, edited by A. Jeffrey (Academic Press, 1994), § 3.944, n. 6), and we have

$$J_{\rm c}(B) = J_{\rm c}(0)\frac{2}{\pi\nu q\sqrt{B}}$$
$$\times\left[1 - 2\sum_{n=1}^{\infty}\frac{\cos\left[(\nu-1){\rm Arctan}\left(2nq\sqrt{B}\right)\right]}{(4n^2-1)(4n^2q^2B)}\right].$$

In the high field region ($B \to \infty$) the sum becomes negligible and the critical current goes to zero as $B^{-1/2}$.

References

1. J.C. Martinez, B. Dam, B. Stauble-Pumpin, G. Doornbos, R. Surdeanu, U. Poppe, R. Griessen, J. Low. Temp. Phys. **105**, 1017 (1996).
2. V. Svetchnikov, V. Pan, Ch. Traeholt, H. Zandbergen, IEEE Trans. Appl. Supercond **7**, 1396 (1997).
3. K.E. Gray, M.B. Field, D.J. Miller, Phys. Rev. B **58**, 9543 (1998).
4. S.K. Streiffer, B.M. Lairson, C.B. Eom *et al.*, Phys. Rev. B **43**, 13007 (1991).
5. B. Dam, J.M. Huijbregste, F.C. Klaassen, R.C.F. van der Geest, G. Doornbos, J.H. Rector, A.M. Testa, S. Freisem, J.C. Martinez, B. Stauble-Punpin, R. Griessen, Nature **399**, 439 (1999).
6. J.M. Huijbregtse, B. Dam, R.C.F. van der Geest, F.C. Klaassen, R. Elberse, J.H. Rector, R. Griessen, Phys. Rev. B **62**, 1338 (2000).
7. L.N. Bulaevskii, J.R. Clem, L.I. Glazman, A.P. Malozemoff, Phys. Rev. B **45**, 2545 (1992).
8. J. Halbritter Phys. Rev. B **48**, 9735 (1993).
9. H. Darhmaoui, J. Jung, Phys. Rev. B **57**, 8009 (1998).
10. E. Mezzetti, R. Gerbaldo, G. Ghigo, L. Gozzelino, B. Minetti, Phys. Rev. B **60**, 7623 (1999), and references therein.
11. G. Ghigo, A. Chiodoni, R. Gerbaldo, L. Gozzelino, B. Minetti, E. Mezzetti, C. Camerlingo, C. Giannini, IEEE Trans. Appl. Supercond. (in press), `arXiv: cond-mat/0005350`.
12. X.Y. Cai, A. Gurevich., I-Fei Tsu, D.L. Kaiser, S.E. Babcock, D.C. Larbalestier, Phys. Rev. B **57**, 10951 (1998).
13. A. Gurevich, M. Friesen, Phys. Rev. B **62**, 4004 (2000).
14. M.V. Fistul', G.F. Giuliani, Phys. Rev. B **51**, 1090 (1995).
15. E. Mezzetti, A. Chiodoni, R. Gerbaldo, G. Ghigo, L. Gozzelino, B. Minetti C. Camerlingo, A. Monaco, Physica C **332**, 115 (2000).
16. A.E. Koshelev, Phys. Rev. B **62**, 3616 (2000).
17. H. Yan, J. Jung, H. Darhmaoui, Z.F. Ren, J.H. Wang, W.K. Kwok, Phys. Rev. B **61**, 11711 (2000).
18. A. Del Vecchio, C. Camerlingo *et al.*, Il Nuovo Cimento D **16**, 2025 (1994).
19. P.E. Di Nunzio, S. Martelli, R. Ricci Bitti, J. Appl. Cryst. **28**, 146 (1995).
20. N.F. Heinig, R.D. Redwing, J.E. Nordman, D.C. Larbalestier, Phys. Rev. B **60**, 1409 (1999).
21. J.R. Clem, B. Bumble, S.I. Raider, W.J. Gallagher, Y.C. Shih, Phys. Rev. B **35**, 6637 (1987).
22. M.A. Itzler, M. Tinkham, Phys. Rev. B **36**, 4003 (1987).
23. A. Daz, L. Mechin, P. Berghuis, J.E. Evetts, Phys. Rev. Lett. **80**, 3855 (1998).
24. G. Rotoli, C. De Leo, G. Ghigo, L. Gozzelino, C. Camerlingo, Int. J. Mod. Phys. B (to be published) .